

A comparative study of different integrate & fire neurons: spontaneous activity, dynamical response, and stimulus-induced correlation

Rafael D. Vilela^{1,2} and Benjamin Lindner¹

¹ *Max-Planck-Institut für Physik Komplexer Systeme, Nöthnitzer Str. 38 01187 Dresden, Germany*

² *Centro de Matemática, Computação e Cognição, Universidade Federal do ABC, 09210-170, Santo André, SP, Brazil*

(Dated: September 30, 2018)

Stochastic integrate & fire (IF) neuron models have found widespread applications in computational neuroscience. Here we present results on the white-noise-driven perfect, leaky, and quadratic IF models, focusing on the spectral statistics (power spectra, cross spectra, and coherence functions) in different dynamical regimes (noise-induced and tonic firing regimes with low or moderate noise). We make the models comparable by tuning parameters such that the mean value and the coefficient of variation of the interspike interval match for all of them. We find that, under these conditions, the power spectrum under white-noise stimulation is often very similar while the response characteristics, described by the cross spectrum between a fraction of the input noise and the output spike train, can differ drastically. We also investigate how the spike trains of two neurons of the same kind (e.g. two leaky IF neurons) correlate if they share a common noise input. We show that, depending on the dynamical regime, either two quadratic IF models or two leaky IFs are more strongly correlated. Our results suggest that, when choosing among simple IF models for network simulations, the details of the model have a strong effect on correlation and regularity of the output.

I. INTRODUCTION

Neurons communicate information via short-lasting discharges of the electrical potential across their membrane. The excitability mechanism by which these spikes are generated relies on the dynamics of voltage-gated ion channels in the neural membrane and is well understood [1, 2]. To study the dynamics of large neural networks, a detailed description of the single neuron's dynamics, although in principle possible, is impractical and one must resort to simpler models of neural spike generation governed by only one or two dynamical variables per neuron [3]. In particular in stochastic versions, that take into account the large variability of neural spiking, these models can be also helpful to study basic aspects of signal transmission by single neurons.

One class of commonly used simplified models comprises integrate & fire (IF) neurons with white noise current. In IF models a spike is generated if the voltage reaches a firing threshold (inducing also a reset of the voltage); the voltage obeys the one-dimensional dynamics

$$\dot{v} = f(v) + s(t) + \mu + \sqrt{2D}\xi(t) \quad (1)$$

where $s(t)$ is a time-dependent stimulus while μ and D are the mean and the noise intensity of the input current ($\xi(t)$ is white Gaussian noise). Variants of the model differ by the function $f(v)$. A fine-tuned choice of $f(v)$ may permit a rather accurate prediction of both experimental subthreshold voltage fluctuations and spike statistics under noisy stimulation *in vitro* and *in vivo* (see [4, 5, 6, 7, 8] for some recent convincing examples). Simple choices like a constant, linear, or quadratic function leading to the perfect (PIF), leaky (LIF), or quadratic (QIF) model, respectively, allow for an analytical calculation of one or the other spike statistics and may be also numerically simpler to simulate in large-scale networks. Models like Eq. (1) have been used in analytical studies of (i) conditions for asynchronous or oscillatory activity in recurrent networks [9, 10, 11, 12]; (ii) the transmission of rapid signals [13, 14, 15, 16]; (iii) the variability of spontaneous

activity [17, 18, 19, 20]; (iv) noise-induced resonances in the spontaneous activity [19, 21], and in the response to external stimuli [14, 22]; and (v) oscillations in recurrent networks induced by spatially correlated stimuli [23, 24, 25], to name but a few.

Most of the phenomena studied depend strongly on the choice of $f(v)$. As an example, consider the effect of coherence resonance, which refers to the existence of an optimal noise intensity D that maximizes the regularity of the spike train, seen, for instance, as a minimum of the coefficient of variation (CV) vs noise intensity: only the leaky [19, 21] but not the perfect or quadratic IF models [20] show such a minimum. It has, furthermore, been shown that LIF and QIF differ strongly in their response to fast (high-frequency) periodic signals [15, 16]. Despite these discussions, however, a systematic comparison among the commonly used IF models is still missing. In this paper, we want to fill this gap.

If one wishes to compare different IF models, the first question is how the input parameters μ and D should be chosen in the respective model. Already the most basic firing statistics of a certain IF model, the firing rate (quantifying the spike train's intensity) and the interspike interval's coefficient of variation (characterizing the variability of the spiking) depend strongly and in a model-specific way on μ and D [17, 19, 20, 26, 27]. The authors have recently shown that this basic firing statistics, i.e. rate and CV, determine uniquely the input parameters μ and D for the three most common IF models mentioned above (perfect, leaky, and quadratic IF neurons). This offers a natural way of unambiguously defining firing regimes for these models. Moreover, setting the firing regime by means of prescribing rate and CV allows for a fair comparison of the higher-order statistics of different IF models. In this way, we can, for example, consider an LIF neuron and a QIF neuron that both show a moderate firing rate (e.g. 10Hz) and medium variability (say, a CV of about 0.5) and compare how these two neurons differ in their spontaneous and driven activity. This approach of assuming the same basic firing statistics and comparing higher-order statistics is complementary to a

previous set-up which was entirely based on the firing rate dependence on input current [15].

What is the most important output statistics of noisy IF neurons once the firing rate and CV are fixed? In most of the above analytical approaches, two single-neuron characteristics appear to be essential: (i) the spike train power spectrum of spontaneous activity and (ii) the response to weak stimuli (e.g. to a weak periodic signal $s(t) = \varepsilon \cos(\omega t)$). In a more recent theory of recurrent networks [25], the knowledge of a third simple property is needed that goes beyond the properties of a single neuron: the degree of correlations that can be induced in two uncoupled neurons that share some common noisy stimulus. This latter property has attracted attention of its own and has been recently studied experimentally (see [28] and references therein) and theoretically [25, 29, 30] in particular in the limit of a weak input correlation.

In the present paper, we study the spontaneous power spectrum, the linear response function (susceptibility), and the two-neuron correlations induced by a common stimulus for the perfect, leaky, and quadratic IF models and a variety of firing regimes. In section II, we introduce the three IF models studied and define the firing regimes. In section III, we present results on spontaneous activity of single neurons. We show that typically IF neurons present similar power spectra when they are in the same firing regime. In section IV, we study the dynamical response of single neurons. We recover characteristic differences between the susceptibility of the LIF and QIF discussed previously (see, e.g. [15]), as well as between LIF and PIF [31], and show in addition that the spectral coherence between spike train and external signal is basically low-pass for all three models. Section V is devoted to the study of two neurons driven in part by common noise. In this case, linear response theory leads to a good approximation for the cross-spectra between the two output spike trains when the common noise makes up only a small fraction of the total noise. Coherence functions of the two output spike trains are again low-pass and resemble qualitatively the input-output coherence functions discussed before. Finally, we discuss the correlation coefficient of the spike count for the LIF and QIF models for a weak common noise and show analytically in the appendix that this correlation coefficient is equal to the input correlation for the PIF model. We summarize our results and draw some conclusions in section VI.

II. MODELS AND FIRING REGIMES

A. Integrate-and-fire neuron models

In this paper we consider IF neurons subjected to stochastic voltage-independent input current, i.e., additive white Gaussian noise which can be justified in the so-called diffusion approximation [26, 32, 33]. We will consider exclusively models driven by white noise, setting the term $s(t)$ in Eq. (1) to zero; a fraction of the input noise will later be regarded as a stimulus or as common noise.

For a leaky integrate-and-fire neuron, the current balance equation reads

$$C_m \dot{V} = -g_L(V - V_L) + \bar{\mu} + \sqrt{2\hat{D}}\xi(t), \quad (2)$$

if $V(t) = V_{th}$ then spike at $t_i = t$ & $V \rightarrow V_r$

where C_m is the capacitance of the cell membrane, g_L and V_L are leak conductance and leak reversal potential, respectively, and $\bar{\mu}$ and \bar{D} are the mean and the intensity of the white Gaussian input noise current. The second line describes the fire-and-reset rule upon reaching the threshold V_{th} .

With the simple transformation $v = (V - V_L)/(V_{th} - V_r)$ and the new parameters $\tau_m = C_m/g_L$ (membrane time constant), $\mu = \bar{\mu}/g_L$, and $\hat{D} = \bar{D}/g_L^2$, this reads

$$\tau_m \dot{v} = -v + \mu + \sqrt{2\hat{D}}\xi(t), \quad (3)$$

if $v(t) = v_{th}$ then spike at $t_i = t$ & $v \rightarrow v_r$

where the threshold and reset are now at $v_{th} = 1$ and $v_r = 0$. When measuring time in multiples of the membrane time constant, i.e. $\hat{t} = t/\tau_m$, this model is equivalent to Eq. (1) with a rescaled noise intensity $D = \hat{D}/\tau_m$ and with $f(v) = -v$. Note that $\mu + \sqrt{2\hat{D}}\xi(t)$ in this rescaled model has not the physical dimensions of an electric current anymore and that is why we will refer to it here with the more general term 'input'.

If the leak term $g_L(V - V_L)$ is small compared to the mean input current, we may be justified to neglect it. All previous transformations can be repeated (including the division by the leak conductance g_L) and thus we end up with

$$\tau_m \dot{v} = \mu + \sqrt{2\hat{D}}\xi(t), \quad (4)$$

if $v(t) = v_{th}$ then spike at $t_i = t$ & $v \rightarrow v_r$

which corresponds after rescaling of time again to Eq. (1) but this time with $f(v) \equiv 0$. This is the perfect integrate-and-fire (PIF) model with white noise (also known as random-walk model of neural firing) [32, 34].

If the noise-free neuron is close to a dynamical bifurcation, specifically, close to a saddle-node bifurcation from quiescence to tonic firing, another form of the integrate-and-fire neuron contains a quadratic nonlinearity [12, 18, 20, 36, 37, 38]

$$C_m \dot{V} = a(V - V_0)^2 + \bar{\mu} + \sqrt{2\hat{D}}\xi(t), \quad (5)$$

if $V(t) = \infty$ then spike at $t_i = t$ & $V \rightarrow -\infty$

In this case one chooses threshold and reset at infinity because the slow dynamics in V makes the exact (large but finite) values of V_r and V_{th} irrelevant. Note also that V in this case can be but has not to be a voltage — in general, it is the variable of the center manifold [38]; correspondingly, the factor C_m on the left-hand-side can be taken as a convention. For infinite reset and threshold values, this dynamics can be brought into a simplified standard form by choosing a new variable $v = a(V - V_0)/g_L$ and new parameters $\mu = a\bar{\mu}/g_L^2$ and $\hat{D} = \bar{D}a^2/g_L^4$:

$$\tau_m \dot{v} = v^2 + \mu + \sqrt{2\hat{D}}\xi(t), \quad (6)$$

if $v(t) = \infty$ then spike at $t_i = t$ & $v \rightarrow \infty$

which corresponds in rescaled time $\hat{t} = t/\tau_m$ and noise intensity $D = \hat{D}/\tau_m$ to Eq. (1) with $f(v) = v^2$. In simulations of this standard form of this quadratic integrate-and-fire neuron (QIF), one uses large but finite threshold

and reset such that – by further increasing their values – the results (ISI statistics, spike train power spectra, etc.) do not change anymore within the desired accuracy (say, curves do not change in line thickness). For the effect of finite values of reset and threshold values on the ISI statistics, see [20].

Note that both in the PIF and the QIF the introduction of the membrane time scale is arbitrary — we could equally well compare to PIF and QIF models in which τ_m would be replaced by a multiple or a fraction of this time (changing then also the input parameters, of course). The choice of τ_m has been made previously for the PIF [44] and we follow here this convention also for the QIF.

Our approach of comparing different IF models here is complementary to others in which the input current is assumed to be known and the parameters of the specific models (e.g. Eq. (2) and Eq. (5)) are fitted to yield a given ISI statistics. Here we start with the standard models Eq. (3), Eq. (4), and Eq. (6) and ask for the input parameters that yield a given rate (in units of the inverse membrane time constant) and a given CV. Although this may seem to be unusual in an experimental situation where one has control over the input current, it appears to be a reasonable approach *in vivo* where the effective input current and its noise intensity is set by the synaptic background and thus unknown.

B. Firing regimes

In order to make different IF models comparable, we must first specify the correspondence between their parameters. For instance, in a comparison between LIF and QIF, we should first decide which pair (D, μ) for the first model corresponds to which pair (D, μ) for the second. Here we do this by defining different firing regimes in terms of fixed rate and coefficient of variation of the spike trains. In other words, D and μ in different models are chosen as to yield a given firing rate

$$r = \frac{1}{\langle T \rangle} \quad (7)$$

and a given coefficient of variation

$$R = \frac{\sqrt{\langle T^2 \rangle - \langle T \rangle^2}}{\langle T \rangle}, \quad (8)$$

where T is the interspike interval. Throughout this paper $\langle \cdot \rangle$ denotes averaging over realizations of the stochastic process. Note that, since time is measured in units of the membrane time constant, all the rates are in units of the inverse of this constant. For instance, for a membrane time constant of 10ms, a nondimensional rate of 1 corresponds to 100Hz.

The pair of parameters (D, μ) for a given model that yields a certain regime is therefore determined by the intersection between one contour line for the rate and one contour line for the CV. However, it is not clear *a priori* whether at most one such intersection exists. This problem was recently addressed by us [39]. We showed that, given fixed rate and CV, there can be at most one associated pair (D, μ) for the three IF models studied in this paper.

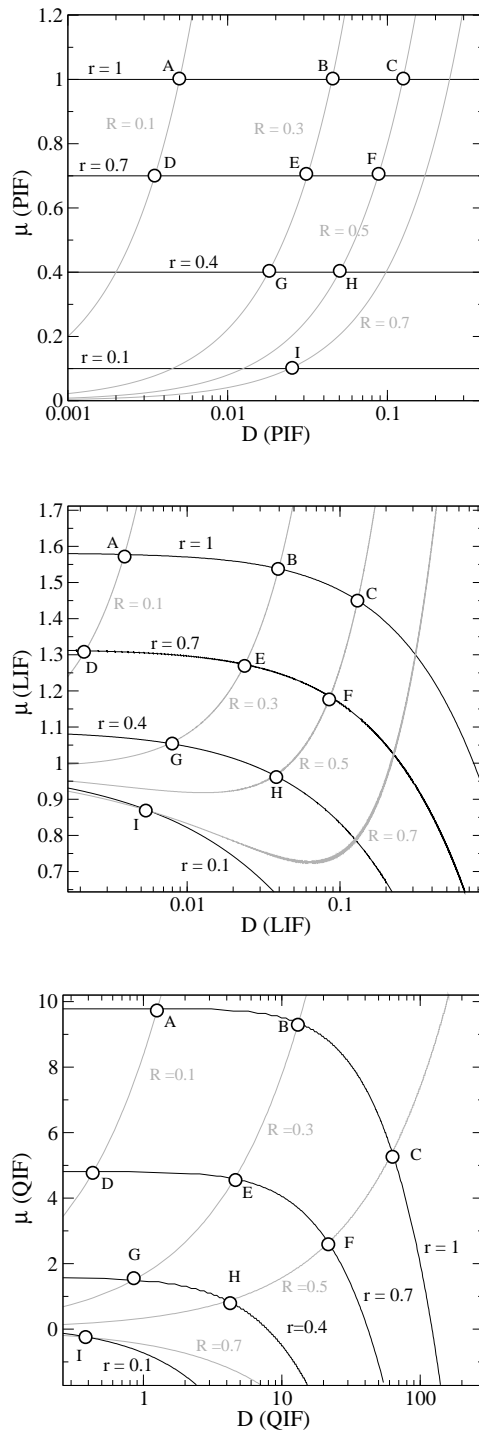


FIG. 1: Contour lines for rate (black) and CV (gray) in parameter space for the different models. Regimes A-I are defined by intersections of these contour lines.

Fig. 1 displays some contour lines for the rate and CV for the three models considered here. There are different ways to determine these contour lines. They can be obtained analytically (see [39]). Here we have determined them numerically, as explained in section III B. In Fig. 1 we also define 9 specific regimes, labeled A-I, which we study in some detail here. The corresponding values for

the rate and CV in these regimes are:

Regime	A	B	C	D	E	F	G	H	I
rate	1	1	1	0.7	0.7	0.7	0.4	0.4	0.1
CV	0.1	0.3	0.5	0.1	0.3	0.5	0.3	0.5	0.7

III. SINGLE NEURONS: SPONTANEOUS ACTIVITY

A. Measures

The output spike train y can be modelled as a sum of delta peaks at the time instants when the voltage described by Eq. (1) reaches the threshold value:

$$y(t) = \sum_j \delta(t - t_j), \quad (9)$$

where t_j is the instant when the j -th spike occurs.

The spontaneous activity of the IF neurons studied here corresponds to a renewal point process. Each interspike interval is an independent random variable. In processes of this type, all the information on the statistics is contained in the probability density of the ISI.

In this paper, we will quantify the neuron's correlation statistics by means of power and cross-spectra. We start by defining the Fourier transform of the zero-average spike train as:

$$\tilde{y}(f) = \int_0^T dt' e^{2\pi i f t'} (y(t') - \langle y(t') \rangle). \quad (10)$$

The power spectrum of the spike train will be the quantity used in this paper to characterize the spontaneous activity of the IF neurons. It is given by:

$$S_y(f) = \lim_{T \rightarrow \infty} \frac{1}{T} \langle \tilde{y} \tilde{y}^* \rangle, \quad (11)$$

where T is the realization time window. For renewal point processes, the relation between the power spectrum of the spike train and the Fourier transform of the probability density of the ISI, $F(f)$, is given by [40]:

$$S_y(f) = \frac{1}{\langle T \rangle} \frac{1 - |F(f)|^2}{|1 - F(f)|^2}. \quad (12)$$

We note that analytical expressions for $F(f)$ are known in the cases of PIF and LIF (equivalently, often the Laplace transform is stated that yields the Fourier transform for a negative imaginary argument). In this work, we will only use that for the PIF, which is given by [31, 41]:

$$F^{(\text{PIF})}(f) = \exp \left[(v_{th} - v_r) \left(\frac{\mu}{2D} - \sqrt{\frac{\mu^2}{4D^2} - \frac{2if\pi}{D}} \right) \right]. \quad (13)$$

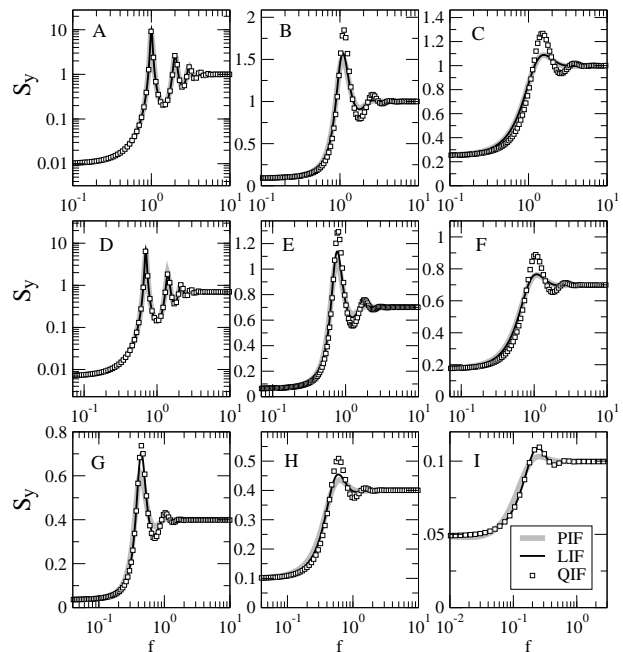


FIG. 2: Power spectra of the spike trains for the three models in the nine firing regimes defined in Fig. 1.

B. Results

In Fig. 2, we show the power spectra for the three models in regimes A-I. These spectra were obtained analytically via Eqs. (12) and (13) for the PIF and numerically for LIF and QIF using the algorithm recently introduced by Richardson [42]. We observe that the power spectra of different models in the same regime are in general very similar. In Regimes A and D, which are characterized by low variability (CV equal to 0.1), the power spectra virtually coincide. In the other regimes, the power spectra coincide in the limits of low and large frequencies, and deviate to some extent in the intermediate-frequency range.

The coincidence of the power spectra for different models in the same regime in the low and large frequency limits is not surprising. In fact, for renewal point processes one can show [40] that:

$$\lim_{f \rightarrow 0} S_y(f) = rR^2 \quad (14)$$

and

$$\lim_{f \rightarrow \infty} S_y(f) = r. \quad (15)$$

Since each regime is defined by fixing the rate and CV, we conclude from Eq. (14) and Eq. (15) that the power spectra for different models should indeed coincide in these limits. In fact, we have used these relations and the above mentioned algorithm for the numerical determination of the power spectrum [42] to obtain the contour lines displayed in Fig. 1.

To quantify the differences between the power spectra of different models, we define the maximal relative difference $\Delta S_y^{j,k}$ between the power spectra of models j and k

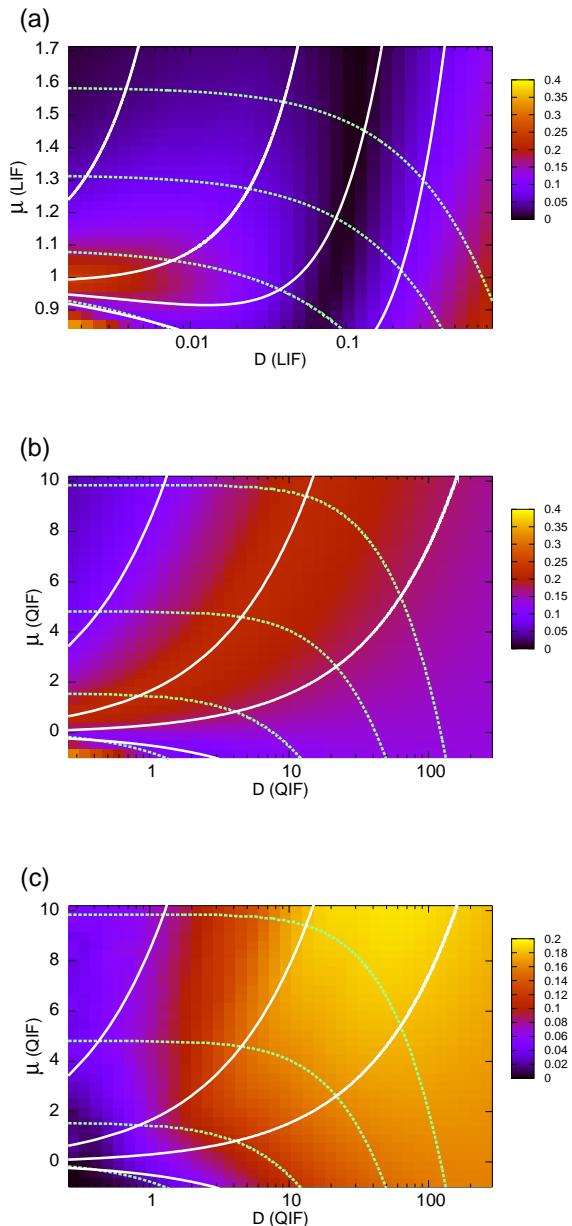


FIG. 3: (Color online) Maximal (over all frequencies) relative difference of power spectra $\Delta S_y^{\text{PIF,LIF}}$ (a), $\Delta S_y^{\text{PIF,QIF}}$ (b), and $\Delta S_y^{\text{LIF,QIF}}$ (c). The contour lines for rate and CV are the same as those depicted in Fig. 1.

over all frequencies as:

$$\Delta S_y^{j,k} = \max_f \left(\frac{|S_y^{(j)} - S_y^{(k)}|}{(S_y^{(j)} + S_y^{(k)})/2} \right). \quad (16)$$

In Fig. 3 we plot $\Delta S_y^{\text{PIF,LIF}}$, $\Delta S_y^{\text{PIF,QIF}}$, and $\Delta S_y^{\text{LIF,QIF}}$. The first observation we make is that the power spectra of the PIF matches those of the LIF and QIF in the parameter regions where the PIF is a good

model, i.e., for large μ and small D [cf. Fig. 3(a) and (b)]. Second, when comparing the LIF with the QIF (Fig. 3(c)), we conclude that the power spectra of these models are practically coincident if the noise intensity is small and their relative difference increases with D , displaying moderate differences for very large noise intensity. There is a nontrivial dependence on μ as well, but the dependence on D is the dominant one. Remarkably, this rule of thumb whereby the power spectra differences between LIF and QIF increase with the noise intensity is valid for both tonic ($\mu_{\text{QIF}} > 0$) and noise-induced ($\mu_{\text{QIF}} < 0$) firing regimes.

IV. SINGLE NEURONS: DYNAMICAL RESPONSE

A. Measures

In this section, we are interested in the response of single neurons to a small stimulus. This can be accomplished in several ways, e.g., by adding a small term with sinusoidal time dependence to Eq. (1). Alternatively, and this is the procedure adopted here, one can regard a fraction of the noise term in Eq. (1) as the external stimulus. This choice will allow for a straightforward connection between the single neuron's response presented in this section and two-neuron correlations under common noise discussed in section V. We thus rewrite Eq. (1) as:

$$\dot{v} = f(v) + \mu + \sqrt{2(1-c)D}\xi_i(t) + \sqrt{2cD}\xi_c(t), \quad (17)$$

where the noise terms $\xi_i(t)$ and $\xi_c(t)$ are white Gaussian and described by:

$$\langle \xi_i(t) \rangle = \langle \xi_c(t) \rangle = \langle \xi_i(t)\xi_c(t') \rangle = 0,$$

$$\langle \xi_c(t)\xi_c(t') \rangle = \langle \xi_i(t)\xi_i(t') \rangle = \delta(t-t'), \quad (18)$$

and c (playing the role of a relative signal amplitude) is a number between 0 and 1. When addressing the single neuron's response, we read Eq. (17) as describing a certain neuron subjected to intrinsic noise $\sqrt{2(1-c)D}\xi_i(t)$ and driven by an external (noisy) stimulus:

$$s(t) = \sqrt{2cD}\xi_c(t). \quad (19)$$

To characterize the neuron's response to the stimulus, we use the cross-spectrum between the spike train y and the stimulus $s(t)$,

$$S_{ys}(f) = \lim_{T \rightarrow \infty} \frac{1}{T} \langle \tilde{y} \tilde{s}^* \rangle, \quad (20)$$

and the coherence function with respect to s ,

$$\gamma^2(f) = \frac{|S_{ys}|^2}{S_y S_s}, \quad (21)$$

where $S_s = 2cD$ is the power spectrum of s . One should note that the coherence function is restricted to the interval $0 < \gamma^2(f) < 1$.

B. Single neuron's response

The cross-spectra (20) can be calculated, for small c , from linear response theory. The idea is to consider the term $\sqrt{2cD}\xi_c$ as a small perturbation of the term μ in the stochastic system

$$\dot{v} = f(v) + \mu + \sqrt{2(1-c)D}\xi_i(t). \quad (22)$$

This does not seem feasible at first sight, since ξ_c has infinitely large variance. To show that linear response can be applied in this case, we formally consider ξ_c as a band pass white noise with flat spectrum of height $2cD$ and cutoff frequency f_{max} . Its variance is then equal to $2cDf_{max}$. This variance can be kept small even in the limit of $f_{max} \rightarrow \infty$ (white noise) if we impose that c decreases sufficiently fast, i.e., $c \ll \mu/2Df_{max}$. Therefore ξ_c can be indeed considered a small perturbation. Linear response theory [43] then leads to the following approximation:

$$\langle \tilde{y}(f) \rangle = \chi_{D,\mu}(f) \sqrt{2cD} \tilde{\xi}_c(f), \quad (23)$$

where $\chi_{D,\mu}$ is the *susceptibility* of the system which can be estimated from the cross spectrum between input signal and spike train via the well-known relation

$$\chi_{D,\mu} = \frac{S_{ys}(f)}{2cD} = \frac{\lim_{T \rightarrow \infty} \langle \tilde{y} \sqrt{2cD} \tilde{\xi}_c^* \rangle_{\xi_i}}{2cD}, \quad (24)$$

Closed analytical forms for χ exist for the PIF [44] and LIF [13, 14], and are given respectively by:

$$\chi_{PIF} = \frac{\mu^2}{v_{th} - v_r} \frac{1 - \sqrt{1 - 8\pi i f D / \mu^2}}{4\pi i f D} \quad (25)$$

and

$$\chi_{LIF} = \frac{r 2\pi i f / \sqrt{D} \mathcal{D}_{2\pi i f - 1} \left(\frac{\mu - v_{th}}{\sqrt{D}} \right) - e^{\delta} \mathcal{D}_{2\pi i f - 1} \left(\frac{\mu - v_r}{\sqrt{D}} \right)}{2\pi i f - 1 \mathcal{D}_{2\pi i f} \left(\frac{\mu - v_{th}}{\sqrt{D}} \right) - e^{\delta} \mathcal{D}_{2\pi i f} \left(\frac{\mu - v_r}{\sqrt{D}} \right)}, \quad (26)$$

where the rate r for the LIF is given by

$$r(\mu, D) = \left(\sqrt{\pi} \int_{(\mu - v_{th})/\sqrt{2D}}^{(\mu - v_r)/\sqrt{2D}} dz e^{z^2} \operatorname{erfc}(z) \right)^{-1}, \quad (27)$$

the abbreviation δ reads

$$\delta = \frac{v_R^2 - v_T^2 + 2\mu(v_{th} - v_r)}{4D}, \quad (28)$$

and $\mathcal{D}_a(z)$ is the parabolic cylinder function [45]. For the QIF, χ can be obtained numerically from the Fokker-Planck equation [46].

C. Results

Since Eq. (24) is valid for arbitrary c , the cross-spectrum S_{ys} is fully characterized by the susceptibility $\chi_{D,\mu}$. We have studied the susceptibility for the three models in regimes A-I. The susceptibility for the PIF was

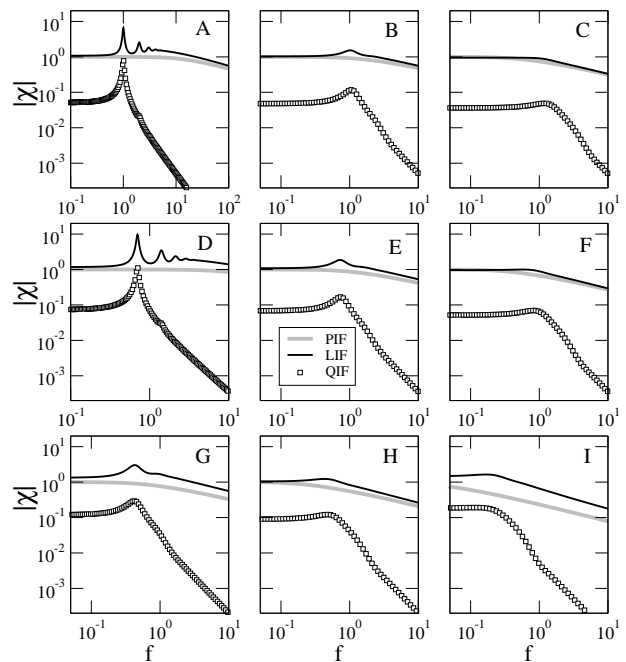


FIG. 4: Gain ($|\chi|$) as a function of frequency for the three models in the Regimes A-I.

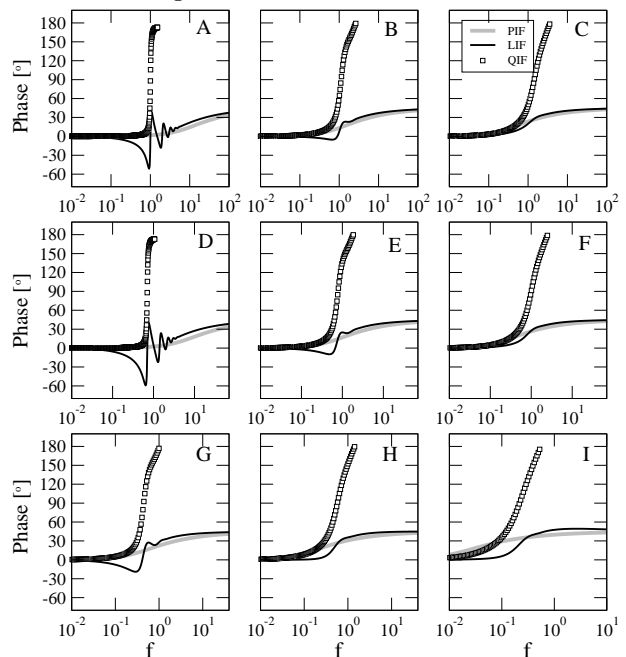


FIG. 5: Phase lag of the linear response (i.e. $-\arg(|\chi|)$) as a function of frequency for the three models in the Regimes A-I. Due to numerical constraints, the phase of the QIF model is not shown in the large frequency range, where it asymptotes to 180° .

determined using Eq. (25), while the susceptibility for the LIF and QIF was determined by integrating the Fokker-Planck equation with the algorithm presented in [42, 46]. It turns out that this numerical integration is faster than the evaluation of Eq. (26) using standard softwares.

In Fig. 4, we show the gain $|\chi|$ as a function of the fre-

quency for the three models in Regimes A-I. The gain is typically larger for the LIF and is in all regimes at least one order of magnitude smaller for the QIF. In regimes A and D, where the firing is most regular, the gain displays peaks for the LIF (close to the firing frequency and its higher harmonics) and QIF (only close to its firing frequency) but not for the PIF. As observed in [15], in the large frequency limit the gain decays as a power law with exponent 0.5 for the LIF and 2 for the QIF. From Eq. (25), we see that the exponent for the PIF is also 0.5.

In Fig. 5, we display the phase ϕ for the different models. It is defined such that $\chi = |\chi|e^{i\phi}$. For the PIF, it is in all regimes close to zero for small frequencies and increases monotonically. Its saturation value, attained in the limit $f \rightarrow \infty$, is $\phi = 45^\circ$. Except for the limits of small and large frequencies, the behavior of the LIF can be markedly different. In particular in Regimes A and D, the phase oscillates around zero in a certain range enclosing the eigenfrequency. It first becomes negative. Close to the eigenfrequency it changes sign, and repeats this oscillatory behavior a few times before approaching its asymptotic value of 45° . Finally, the behavior of the phase for the QIF is similar to the one of the LIF, except that the asymptotic value at large frequencies is remarkably larger - equal to 180° . The asymptotic behaviors for the LIF and QIF were also discussed in [15].

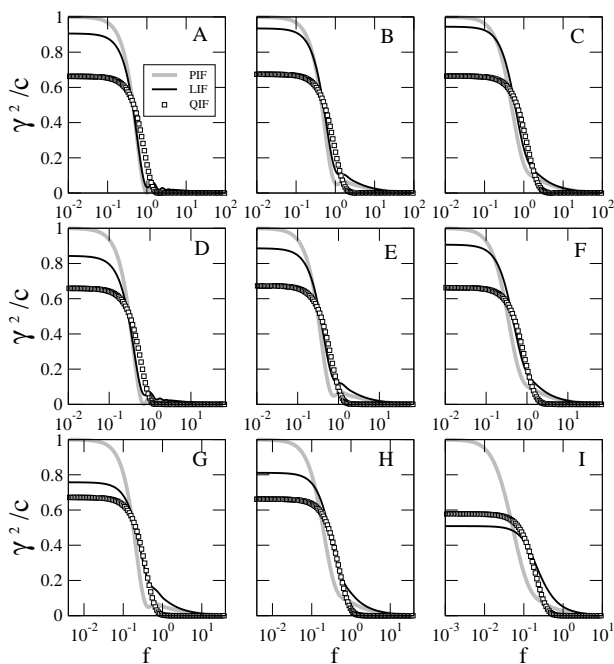


FIG. 6: Coherence function γ^2 for the three models in the Regimes A-I. Note that, in Regime I, the coherence of the QIF is larger than that of LIF for small frequencies.

We now turn to the coherence function γ^2 that we show in multiples of c for the different models in Fig. 6. Although the gain of the three models differed by more than one order of magnitude and showed different resonances, their coherence functions are rather similar and display a low-pass behavior. Therefore PIF, LIF, and QIF transmit most information in a low-frequency band of the stimulus. Going to the limit of vanishing frequencies, the PIF will transmit most information: as can be

explicitly shown [31], γ^2 for the PIF approaches the maximum value c in the limit of zero frequency, a feature not shared by neither LIF nor QIF. Furthermore, the coherence function at low frequencies can be larger for the LIF as compared to the QIF (regimes A-H) and, conversely, larger for the QIF as compared to the LIF (regime I). As we will argue in the next section, this feature also affects which of these models will display larger two-neuron correlations under common noise stimulus.

V. TWO-NEURON CORRELATIONS UNDER COMMON STIMULUS

A. Measures

We now study two neurons of the same model subjected to individual noise and also to common noise. For this purpose we consider the following modification of Eq. (17):

$$\dot{v}_i = f(v_i) + \mu + \sqrt{2(1-c)D}\xi_i(t) + \sqrt{2cD}\xi_c(t), \quad (29)$$

where the subscript i stands for the neuron's index and can attain the values 1 and 2. Eqs. (18) remain valid, and we now also have:

$$\langle \xi_1(t)\xi_2(t') \rangle = 0. \quad (30)$$

To characterize the correlations between the output spike trains of two different neurons, we will use their cross-spectrum,

$$S_{y_1 y_2}(f) = \lim_{T \rightarrow \infty} \frac{1}{T} \langle \tilde{y}_1 \tilde{y}_2^* \rangle, \quad (31)$$

and their coherence function,

$$\Gamma^2(f) = \frac{|S_{y_1 y_2}|^2}{S_{y_1} S_{y_2}}. \quad (32)$$

Another important measure of correlation between two spike trains is the correlation coefficient of the spike count. The spike counts n_1 and n_2 are the numbers of spikes elicited by neurons 1 and 2, respectively, over a time window of length T . Their correlation coefficient is defined as:

$$\rho_T = \frac{\langle n_1 n_2 \rangle - \langle n_1 \rangle \langle n_2 \rangle}{\sqrt{\langle n_1^2 \rangle - \langle n_1 \rangle^2} \sqrt{\langle n_2^2 \rangle - \langle n_2 \rangle^2}} \quad (33)$$

and its range lies between -1 and 1. In the important limit of large time windows, one can prove the following relation between this correlation coefficient and the zero frequency values of the cross- and power-spectra of the spike train [28]:

$$\rho \equiv \lim_{T \rightarrow \infty} \rho_T = \lim_{f \rightarrow 0} \frac{S_{y_1 y_2}(f)}{\sqrt{S_{y_1}(f) S_{y_2}(f)}}. \quad (34)$$

B. Small input correlation

We now calculate $S_{y_1 y_2}(f)$ in the case of small c . Using Eq. (23), we obtain:

$$S_{y_1 y_2}(f) = \lim_{T \rightarrow \infty} \frac{1}{T} \langle \langle \tilde{y}_1 \tilde{y}_2^* \rangle_{\xi_1} \rangle_{\xi_2} \rangle_{\xi_c} =$$

$$\lim_{T \rightarrow \infty} \frac{1}{T} \langle \langle \tilde{y}_1 \rangle_{\xi_1} \langle \tilde{y}_2^* \rangle_{\xi_2} \rangle_{\xi_c} = 2cD |\chi_{D, \mu}|^2, \quad (35)$$

where the averages were taken first over ξ_1 (with frozen ξ_2 and ξ_c), then over ξ_2 (with frozen ξ_c), and finally over realizations of ξ_c . Eq. (35) has been already used in the literature [24, 25].

Since the limit of χ at zero frequency is given by $\frac{dr}{d\mu}$, for small input correlation Eq. (34) has the simple form [28]:

$$\rho = \frac{2cD \left| \frac{dr}{d\mu} \right|^2}{rR^2}. \quad (36)$$

Eqs. (21), (24), (34), and (35) imply that, for small c , the correlation coefficient of the spike count is equal to the limit value of the coherence function γ^2 at zero frequency.

C. Results

Our analysis of the two-neuron correlation relies primarily on simulations of the stochastic differential equations (Eq. (29)) and the evaluation of the cross-spectra (Eq. (31)). This is computationally considerably more demanding than the simple integration of the Fokker-Planck equation and the evaluation of the analytical expressions leading to the results presented in the previous sections. For this reason we now restrict ourselves to the analysis of regimes C and I only. However, this suffices to lead us to three important conclusions, which we now state. First, as Figs. 7 and 8 show, linear response theory leads to good approximations for the cross-spectra $S_{y_1 y_2}$ for small c (e.g., $c=0.1$). Second, we note from Fig. 9 that, as the input correlation c approaches 1, the convergence of $S_{y_1 y_2}$ to S_y and of $\Gamma^2(f)$ to the maximum value 1 (for all f) is very slow. This convergence is more pronouncedly slow for large frequencies, which corresponds to the fact that a tiny amount of individual noise is enough to produce a finite difference in the spiking times of the two neurons. Third, the coherence function in the important limit of small frequencies is larger for the LIF in regime C as compared to the QIF and, conversely, larger for the QIF as compared to the LIF in regime I.

In view of the discussion in section V A, we conclude that the correlation coefficient ρ of the spike count in the limit of large time windows is larger for the LIF than for the QIF in regime C and larger for the QIF than for the LIF in regime I. In Fig. 10, this is shown to occur for c in the whole range $0 \leq c \leq 1$. We also observe that an approximately linear dependence holds in a fairly broad range in Regimes C and I for both models.

Regime C

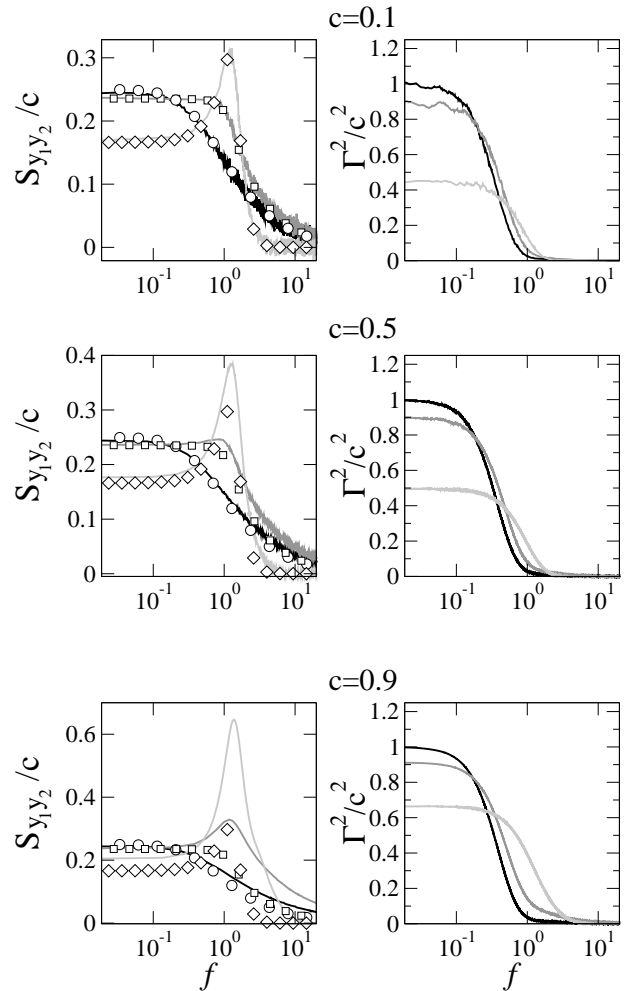


FIG. 7: Cross-spectra between the two output spike trains of neurons under common noise stimulus divided by the input correlation c (left panels) and coherence function of the two output spike trains divided by c^2 (right panels) in Regime C. PIF (black), LIF (dark gray), and QIF (light gray) are compared. In the left panels, the circles (PIF), squares (LIF), and diamonds (QIF) correspond to the prediction from Eq. (35).

In order to provide a complete picture of the correlation coefficient not only for two specific regimes but rather in a fairly broad region of the parameter space, we show in Fig. 11 and Fig. 12 the ratio ρ/c as a function of μ and D for the LIF and QIF, respectively. They were estimated on the basis of the Eq. (36) and are expected to be correct for small input correlation c . For the LIF, we have calculated the terms in Eq. (36) from the exact analytical expressions (see e.g. [39]). For the QIF we resorted to the numerical algorithm of Refs. [46] and [42].

We note from that for both LIF and QIF the correlation coefficient falls sharply when the Poissonian firing regime (low D and μ) is approached. Also remarkable is the fact that, at least in the studied parameter regions, the correlation coefficient for the LIF can approach 1 (if

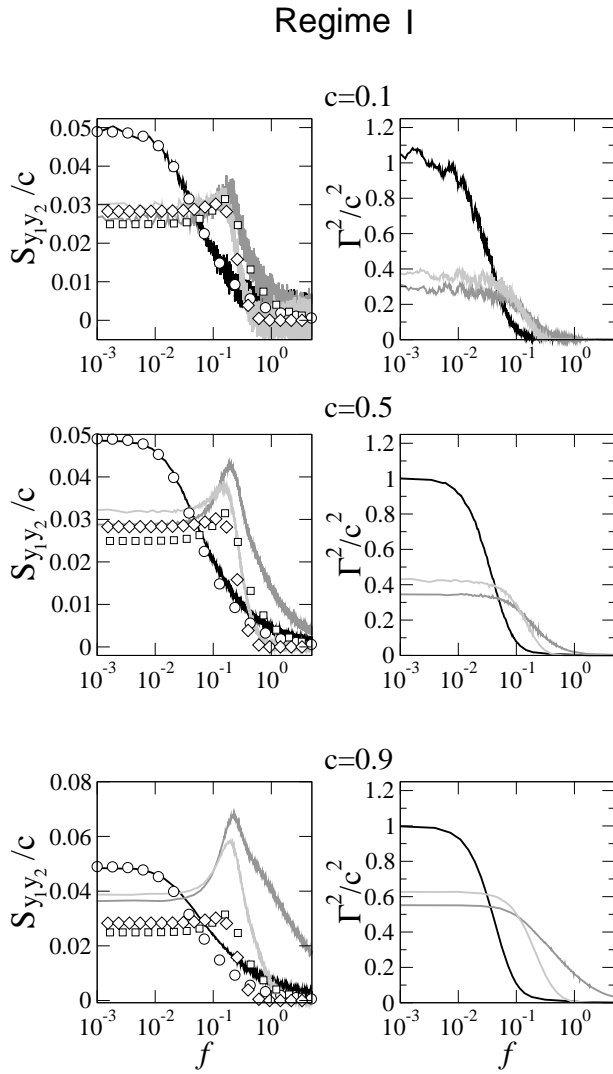


FIG. 8: Cross-spectra between the two output spike trains of neurons under common noise stimulus divided by the input correlation c (left panels) and coherence function of the two output spike trains divided by c^2 (right panels) in Regime I. PIF (black), LIF (dark gray), and QIF (light gray) are compared. In the left panels, the circles (PIF), squares (LIF), and diamonds (QIF) correspond to the prediction from Eq. (35).

μ and D are large), but the correlation coefficient for the QIF seems to have a considerably smaller upper bound (below 0.7). Let us now describe some simple limits of ρ/c . For the QIF, this quantity approaches the value $2/3$ in the limit of strong input ($\mu > 0$) and weak noise ($D \ll 1$). In the excitable regime ($\mu < 0$) at weak noise ($D \ll |\mu|^{3/2}$), i.e., when the firing is close to Poissonian, ρ/c approaches zero.

In Fig. 13, we show the ratio between the correlation coefficients of LIF and QIF. The correlation coefficient is larger for the LIF in most parts of the analyzed parameter space. Only when μ and D are small, i.e., when the firing is close to Poissonian, is the correlation coefficient larger for the QIF than for the LIF.

Finally we turn to the simplest case of the PIF. For this model, one can show that the correlation coefficient

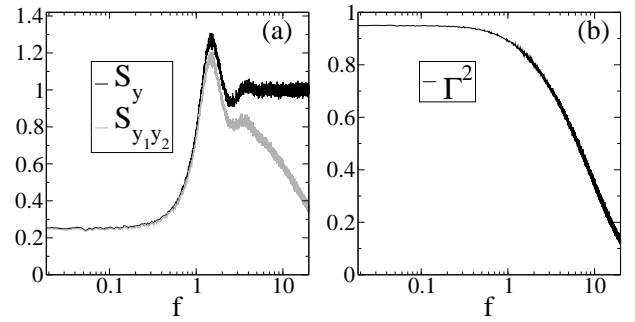


FIG. 9: Power- and cross-spectra of the output spike trains of two QIF neurons under common noise stimulus (a) and coherence function of the two output spike trains (b) in Regime C for $c = 1 - \epsilon$, with $\epsilon = 10^{-3}$.

is given simply by c . In the terminology introduced in [28], the correlation susceptibility is equal to 1 for the PIF. Using Eq. (35), we obtain

$$\rho^{(\text{PIF})} = \lim_{f \rightarrow 0} \frac{2cD|\chi(f)|^2}{S_y(f)}. \quad (37)$$

Using Eqs. (21) and (24), as well as the fact that $\lim_{f \rightarrow 0} \gamma^2(f) = 1$ for the PIF (see [31]), we obtain

$$\rho^{(\text{PIF})} = c. \quad (38)$$

Remarkably, this linear law, in principle valid only for small c , can be shown for the PIF to be valid for all $c \in [0, 1]$, as we show in the Appendix.

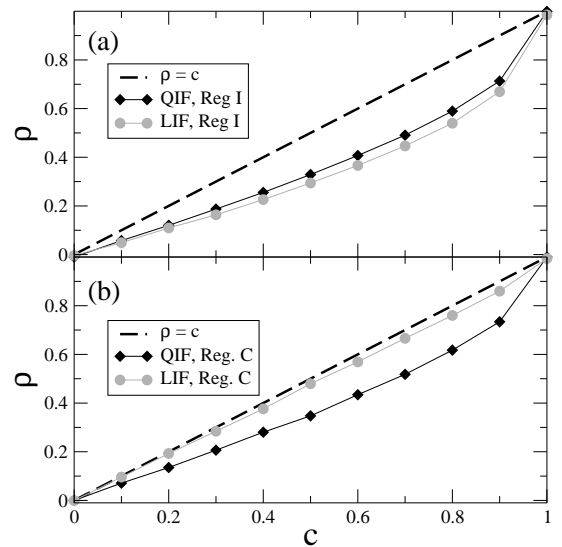


FIG. 10: Correlation coefficient of the spike count vs input correlation for large time window for LIF and QIF in firing regimes I (a) and C (b).

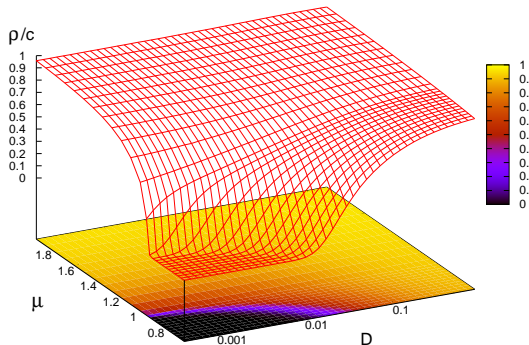


FIG. 11: (Color online) Correlation coefficient (divided by c) of the spike counts at large time windows for the LIF as a function of both D and μ .

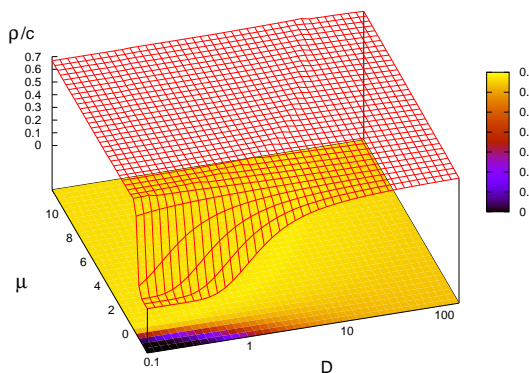


FIG. 12: (Color online) Correlation coefficient (divided by c) of the spike counts at large time windows for the QIF as a function of both D and μ .

VI. CONCLUSIONS

We have provided an extensive comparison of three important IF models in different firing regimes, as determined by given firing rate and CV. We have shown that the spontaneous activity of the LIF and QIF neurons virtually coincide in regimes characterized by weak input noise and deviates moderately for larger values of the input noise. The dynamical response behavior, however, strongly differs among different models, even in the same firing regimes. This was discussed in the limit of large stimulus frequencies in [15] and extended here for the entire frequency range.

An important feature of the single neuron's response characteristics is that, depending on the firing regime, it can be stronger at a given frequency for the LIF as compared to the QIF or the other way around. We have shown that this implies, as long as the linear response theory holds true (i.e., for small c), that either two LIF or two QIF neurons can display larger low-frequency correlations when driven in part by common noise. Altogether our findings indicate that the successful use of a

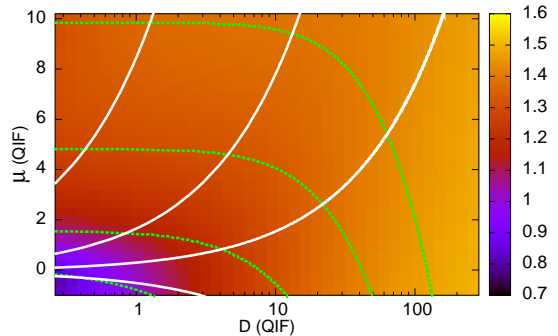


FIG. 13: (Color online) Ratio between the correlation coefficients of the spike counts of LIF and QIF in the limit of large time windows. The contour lines for rate and CV are the same as those depicted in Fig. 1.

certain IF model to reproduce the spontaneous activity of biological neurons does not at all guarantee that the correlations in the activity of a population of such neurons will be also well described. More important for the latter are the dynamical response characteristics of the single neuron to an external stimulus.

We have also characterized a large portion of the physiologically relevant parameter space of the studied IF models and concluded that the correlations in the spike trains of two LIFs, as characterized by the correlation coefficient for the spike count, are in most cases larger than the corresponding correlations of two QIFs. An important exception, however, exists: when the firing approaches the Poissonian regime, the correlations between QIF neurons become larger than those of two LIF neurons.

It constitutes an interesting open problem to perform the same studies as done here for other IF models, e.g. the exponential IF model introduced in [15]. Finally, an extensive comparison between type I [18, 20, 47] and type II [48, 49, 50] neurons as regards to spontaneous activity, dynamical response, and two-neuron correlation under common stimulus is still lacking and is expected to shed light on the problem of how large neuronal populations encode and transmit information.

VII. ACKNOWLEDGMENT

We would like to thank Magnus J. E. Richardson for help on his algorithm from [42] prior to publication.

APPENDIX A: CORRELATION COEFFICIENT FOR THE PIF FOR ARBITRARY c

Here we show that the correlation coefficient for the PIF is for an input correlation $c \in [0, 1]$ given by:

$$\rho^{(\text{PIF})} = c. \quad (\text{A1})$$

For this purpose, we track the *non-reset* voltage of the PIF described by:

$$\dot{v}_i = \mu + \sqrt{1 - c}\xi_i(t) + \sqrt{c}\xi_c(t), \quad (\text{A2})$$

and observe that, in the limit of large times, the relative error in approximating the spike count $n_i(t)$ by this unresetted voltage $v_i(t)$ approaches zero, i.e.:

$$\lim_{t \rightarrow \infty} \frac{n_i(t) - v_i(t)}{(n_i(t) + v_i(t))/2} = 0. \quad (\text{A3})$$

Eq. (A3) holds true because the difference between the spike count and the non-reset voltage is a number between 0 and 1 (assuming $v_{th} - v_r = 1$). In other words, the numerator appearing in the limit of Eq. (A3) remains bounded between 0 and 1 for all t , while the denominator goes to infinity as $t \rightarrow \infty$.

Approximating the spike count $n_i(t)$ by this unresetted voltage $v_i(t)$, we obtain an alternative formula for the correlation coefficient for the spike count of the PIF:

$$\rho^{(\text{PIF})} = \lim_{t \rightarrow \infty} \frac{\langle v_1(t)v_2(t) \rangle - \langle v_1(t) \rangle \langle v_2(t) \rangle}{\sqrt{(\langle v_1^2(t) \rangle - \langle v_1(t) \rangle^2)(\langle v_2^2(t) \rangle - \langle v_2(t) \rangle^2)}}. \quad (\text{A4})$$

To calculate the right-hand side of Eq. (A4), we use the formal solution of Eq. (A2), given by:

$$v_i(t) = \int_0^t (\mu + \sqrt{1 - c}\xi_i(t') + \sqrt{c}\xi_c(t')) dt'. \quad (\text{A5})$$

Substituting Eq. (A5) in Eq. (A4) and using Eqs. (18) and (30), we obtain Eq. (A1).

APPENDIX B: NUMERICAL METHODS

The contour lines for the rate for both LIF and QIF, as well as the respective power spectra, were obtained by resorting to the numerical algorithm of Ref. [42]. For the LIF (QIF), the rate and CV were calculated for the points on a roughly 2000×2000 ($10^3 \times 10^3$) grid over the (D, μ) region displayed in Fig. 1. The integration step for the numerical evaluation of the Fokker-Planck equation (see [42]) was equal to 10^{-4} for the LIF and 10^{-3} for the QIF, with the threshold and reset at $\pm\infty$ being numerically replaced by ± 500 for the latter. The CV was estimated by assuming that the power spectrum at a frequency 10^3 times smaller than the firing rate was equal to rR^2 (see Eq. (14)) for both LIF and QIF.

The gain and phase for the linear response of LIF and QIF were computed using the algorithm of Ref. [46], with the same integration steps (as well as reset and threshold values for the QIF) as above. Finally, the cross-spectra $S_{y_1 y_2}$ were obtained from a fast Fourier transform algorithm after integrating the stochastic differential equations Eq. (29) with a time step of 10^{-3} . For the LIF, a correction based on the probability that the voltage reached the threshold and decreased below it within the time interval dt was implemented (see [51]).

-
- [1] B. Hille. *Ion channels of excitable membranes*. Sinauer, Sunderland, 2001.
- [2] C. Koch. *Biophysics of Computation - Information Processing in Single Neurons*. Oxford University Press, New York, Oxford, 1999.
- [3] W. Gerstner and W. Kistler. *Spiking Neuron Models*. Cambridge, Cambridge, UK, 2002.
- [4] L. Badel, S. Lefort, R. Brette, C. C. H. Petersen, W. Gerstner, and M. J. E. Richardson. Dynamic I-V curves are reliable predictors of naturalistic pyramidal-neuron voltage traces. *J. Neurophysiol.*, 99:656, 2008.
- [5] R. Jolivet, R. Kobayashi, A. Rauch, R. Naud, S. Shinomoto, and W. Gerstner. A benchmark test for a quantitative assessment of simple neuron models. *J. Neurosci. Methods*, 169:417, 2008.
- [6] R. Jolivet, F. Schurmann, T. K. Berger, R. Naud, W. Gerstner, and A. Roth. The quantitative single-neuron modeling competition. *Biol. Cybern.* 99:417, 2008.
- [7] A. Rauch, G. La Camera, H. R. Luscher, W. Senn, and S. Fusi. Neocortical pyramidal cells respond as integrate-and-fire neurons to in vivo-like input currents. *J. Neurophysiol.*, 90:1598, 2003.
- [8] P. Lansky, P. Sanda, and J. F. He. The parameters of the stochastic leaky integrate-and-fire neuronal model. *J. Comput. Neurosci.* 21:211, 2006.
- [9] L. F. Abbott and C. van Vreeswijk. Asynchronous states in a network of pulse-coupled oscillators. *Phys. Rev. E*, 48:1483, 1993.
- [10] D. J. Amit and N. Brunel. Dynamics of a recurrent network of spiking neurons before and following learning. *Network: Comput. Neural Syst.*, 8:373, 1997.
- [11] N. Brunel. Dynamics of sparsely connected networks of excitatory and inhibitory spiking neurons. *J. Comput. Neurosci.*, 8:183, 2000.
- [12] D. Hansel and G. Mato. Existence and stability of persistent states in large neuronal networks. *Phys. Rev. Lett.*, 86:4175, 2001.
- [13] N. Brunel, F. S. Chance, N. Fourcaud, and L. F. Abbott. Effects of synaptic noise and filtering on the frequency response of spiking neurons. *Phys. Rev. Lett.*, 86:2186, 2001.
- [14] B. Lindner and L. Schimansky-Geier. Transmission of noise coded versus additive signals through a neuronal ensemble. *Phys. Rev. Lett.*, 86:2934, 2001.
- [15] N. Fourcaud-Trocmé, D. Hansel, C. van Vreeswijk, and N. Brunel. How spike generation mechanisms determine the neuronal response to fluctuating inputs. *J. Neurosci.*, 23:11628, 2003.
- [16] B. Naundorf, T. Geisel, and F. Wolf. Dynamical response properties of a canonical model for type-I membranes. *Neurocomputing*, 65:421, 2005.
- [17] L. M. Ricciardi and L. Sacerdote. The Ornstein-Uhlenbeck process as a model for neuronal activity. *Biol. Cybernetics*, 35:1, 1979.
- [18] B. S. Gutkin and G. B. Ermentrout. Dynamics of membrane excitability determine interspike interval variability: A link between spike generation mechanisms and cortical spike train statistics. *Neural Comp.*, 10:1047, 1998.

- [19] B. Lindner, L. Schimansky-Geier, and A. Longtin. Maximizing spike train coherence or incoherence in the leaky integrate-and-fire model. *Phys. Rev. E*, 66:031916, 2002.
- [20] B. Lindner, A. Longtin, and A. Bulsara. Analytic expressions for rate and CV of a type I neuron driven by white Gaussian noise. *Neural. Comp.*, 15:1761, 2003.
- [21] K. Pakdaman, S. Tanabe, and T. Shimokawa. Coherence resonance and discharge reliability in neurons and neuronal models. *Neural Networks*, 14:895, 2001.
- [22] M. Stemmler. A single spike suffices: the simplest form of stochastic resonance in neuron models. *Network*, 7:687, 1996.
- [23] B. Doiron, M. J. Chacron, L. Maler, A. Longtin, and J. Bastian. Inhibitory feedback required for network burst responses to communication but not to prey stimuli. *Nature*, 421:539, 2003.
- [24] B. Doiron, B. Lindner, A. Longtin, L. Maler, and J. Bastian. Oscillatory activity in electrosensory neurons increases with the spatial correlation of the stochastic input stimulus. *Phys. Rev. Lett.*, 93:048101, 2004.
- [25] B. Lindner, B. Doiron, and A. Longtin. Theory of oscillatory firing induced by spatially correlated noise and delayed inhibitory feedback. *Phys. Rev. E*, 72:061919, 2005.
- [26] L. M. Ricciardi. *Diffusion Processes and Related Topics on Biology*. Springer-Verlag, Berlin, 1977.
- [27] A. N. Burkitt. A review of the integrate-and-fire neuron model: I. homogeneous synaptic input. *Biol. Cyber.*, 95:1, 2006.
- [28] J. de la Rocha, B. Doiron, E. Shea-Brown, K. Josic, and A. Reyes. Correlation between neural spike trains increases with firing rate. *Nature*, 448:802, 2007.
- [29] E. Salinas and T. J. Sejnowski. Correlated neuronal activity and the flow of neural information. *Nature Rev. Neurosci.*, 2:539, 2001.
- [30] E. Shea-Brown, K. Josic, J. de la Rocha, and B. Doiron. Correlation and synchrony transfer in integrate-and-fire neurons: basic properties and consequences for coding. *Phys. Rev. Lett.*, 100:108102, 2008.
- [31] R. B. Stein, A. S. French, and A. V. Holden. The frequency response, coherence, and information capacity of two neuronal models. *Biophys. J.*, 12:295, 1972.
- [32] A. V. Holden. *Models of the Stochastic Activity of Neurons*. Springer-Verlag, Berlin, 1976.
- [33] H. C. Tuckwell. *Stochastic Processes in the Neuroscience*. Society for industrial and applied mathematics, Philadelphia, Pennsylvania, 1989.
- [34] G. L. Gerstein and B. Mandelbrot. Random walk models for the spike activity of a single neuron. *Biophys. J.*, 4:41, 1964.
- [35] P.I.M. Johannesma. Diffusion models of the stochastic activity of neurons. In E.R. Caianiello, editor, *Neural Networks*, page 116. Springer, Berlin, 1968.
- [36] G. B. Ermentrout. Type I membranes, phase resetting curves, and synchrony. *Neural. Comp.*, 8:979, 1996.
- [37] P. E. Latham, B. J. Richmond, P. G. Nelson and S. Nirenberg. Intrinsic Dynamics in neuronal networks. I. Theory. *J. Neurophysiol.* 83:808, 2000.
- [38] E. M. Izhikevich. *Dynamical Systems in Neuroscience: The Geometry of Excitability and Bursting* (The MIT Press, Cambridge, London, 2007).
- [39] R. D. Vilela and B. Lindner. Are the input parameters of white-noise-driven integrate & fire neurons uniquely determined by rate and cv? *J. Theor. Biol.*, 257:90, 2009.
- [40] D. R. Cox and P. A. W. Lewis. *The Statistical Analysis of Series of Events*. Chapman and Hall, London, 1966.
- [41] H. Sugiyama, G. P. Moore, and D. H. Perkel. Solutions for a stochastic model of neuronal spike production. *Math. Biosci.*, 8:323, 1970.
- [42] M. J. E. Richardson. Spike-train spectra and network response functions for non-linear integrate-and-fire neurons. *Biological Cybernetics*, 99:381, 2008.
- [43] H. Risken. *The Fokker-Planck Equation*. Springer, Berlin, 1984.
- [44] N. Fourcaud and N. Brunel. Dynamics of the firing probability of noisy integrate-and-fire neurons. *Neural Comp.*, 14:2057, 2002.
- [45] M. Abramowitz and I. A. Stegun. *Handbook of Mathematical Functions*. Dover, New York, 1970.
- [46] M. J. E. Richardson. Firing-rate response of linear and nonlinear integrate-and-fire neurons to modulated current-based and conductance-based synaptic drive. *Phys. Rev. E*, 76:021919, 2007.
- [47] J. Rinzel and B. Ermentrout. Analysis of neural excitability and oscillations. In C. Koch and I. Segev, editors, *Methods in Neuronal Modeling: From Ions to Networks*, page 251. MIT Press, Cambridge, Mass., 1989.
- [48] E. M. Izhikevich. Resonate-and-fire neurons. *Neural Networks*, 14:883, 2001.
- [49] N. Brunel, V. Hakim, and M. J. E. Richardson. Firing-rate resonance in a generalized integrate-and-fire neuron with subthreshold resonance. *Phys. Rev. E*, 67:051916, 2003.
- [50] M. J. E. Richardson, N. Brunel, and V. Hakim. From subthreshold to firing-rate resonance. *J. Neurophysiol.*, 89:2538, 2003.
- [51] B. Lindner and A. Longtin. Effect of an exponentially decaying threshold on the firing statistics of a stochastic integrate-and-fire neuron. *J. Theor. Biol.* 232:505 (2005).